Sensitivity of Observationally Based Estimates of Ocean Heat Content and Thermal Expansion to Vertical Interpolation Schemes

Yuehua Li[1,2,3], John A. Church[1], Trevor J. McDougall[2], Paul M. Barker[2]

1. Climate Change Research Centre, University of New South Wales, Sydney, Australia.
2. School of Mathematics, University of New South Wales, Sydney, Australia.
3. School of Earth Science, Yunnan University, Kunming, China

Corresponding author:

John Church. John.Church@UNSW.edu.au

Key points:

- Estimates of upper ocean warming from 1956 to 2020 with an improved vertical interpolation method are 14% larger than linear interpolation schemes.
- The corresponding upper ocean thermal expansion is 14% larger than linear interpolation.
- The greater ocean heat storage and thermal expansion discrepancies occur at 15ºN and 12ºS, near the maxima in the curvature of the temperature depth profile.

Abstract:

Changes in ocean heat content are a critical element of climate change, with the oceans containing about 90% of the excess heat stored in the climate system (60% in the upper 700 db). Estimates of these changes are sensitive to horizontal mapping of the sparse historical data and errors in eXpendable BathyThermograph data. Here we show that they are also sensitive to the vertical interpolation of sparsely sampled data through the water column. We estimate, using carefully constructed vertical interpolation methods with high-quality hydrographic (bottle and CTD) data, the observationally based upper ocean heat content increase (thermosteric sea level rise) from 1956 to 2020 is 285 Zeta Joules (0.55 mm yr^{-1}), 14% (14%) larger than estimates relying on simple but biased linear interpolation schemes. The underestimates have a clear spatial pattern with their maximum near 15ºN and 12ºS, near the maxima in the curvature of the temperature depth profile.

Plain Language Summary:

Change in ocean heat content is a critical element of anthropogenic climate change, with the oceans containing about 90% of the excess heat stored in the climates system, and 60% of this in the upper ocean (0 to 700 db). We estimate, using carefully constructed vertical interpolation methods with high-quality hydrographic (bottle and CTD) data, that the upper ocean heat content increase (thermosteric sea level rise) from 1956 to 2020 is 285 Zeta Joules (0.55 mm yr^{-1}), 14% (14%) larger than estimates relying on simple but biased linear interpolation schemes. The underestimates caused by linear interpolation of ocean heat storage (thermosteric sea-level rise) have a clear spatial pattern with their maximum near 15º N and 12º S near the location with the maxima in the curvature of the temperature depth profile.

Key Words: Climate change, global warming, ocean heat content, sea level rise

1. Introduction

The global energy balance is a fundamental aspect of the Earth's climate. Increasing greenhouse gas and aerosol concentrations (and smaller variations from solar and volcanic changes) have been increasing the effective radiative forcing of the Earth. This energy inflow is balanced by about two thirds leaving the Earth system as long-wave radiation and about a third absorbed within the climate system (Murphy et al., 2009; Trenberth and Fusullo, 2010; Church et al., 2011, 2013a,b; Stevens et al., 2012; von Schuckmann et al., 2016). Most of this stored energy since the 1950s (89-94%) is in the ocean (Levitus et al., 2001, Church et al., 2011, updated 2013a, 2013b; Rhein et al., 2013, Forster et al., 2021; von Schuckmann et al., 2020), with about 60% of the ocean storage in the upper 700 db (von Schuckmann et al., 2020).

Early studies using a combination of high-quality research-ship, and lower quality expendable bathythermograph (XBT) observations reported an apparent decadal oscillation in upper-ocean heat storage (Levitus et al., 2005; Ishii et al., 2005; Bindoff et al., 2007), a result of significant (warm) biases in the XBT data (Gouretski and Koltermann, 2007). Corrections to the XBT fall rate (Wijffels et al., 2008) and/or the XBT temperatures (Levitus et al., 2009; Ishii et al., 2009) reduced this oscillation and the resultant upper-ocean heat content are in better agreement with model simulations (Domingues et al., 2008). Significant differences between various XBT corrections remain (Cheng et al., 2018). Studies have also explored the impact of different lateral mapping techniques and XBT corrections (Boyer et al., 2016; Savita et al., 2021). The advent of the uniformly high-quality Argo data (Gould et al., 2004) has reduced the uncertainties associated with mapping techniques and instrumental biases and

resulted in improved estimates of ocean heat storage from the surface to 2000 db since 2006 (Roemmich et al., 2015; Wijffels et al., 2016; Johnson et al., 2016).

Uncertainties in ocean heat content associated with sparse sampling in the vertical has not received much attention in recent years, with most groups either using some form of the vertical interpolation scheme proposed by Reiniger and Ross (1968; hereafter RR) or linear interpolation (LIN). However, Cheng and Zhou (2014b) have identified biases and uncertainties in ocean heat content as a result of sparse vertical sampling in historical data, acting in conjunction with the curvature of the temperature profile with depth.

Barker and McDougall (2020) proposed a new interpolation scheme using Multiply-Rotated Piecewise Cubic Hermite Interpolating Polynomials (MR-PCHIP). This method is better at interpolating sparse historical data without the artificial production of anomalous water masses or the unrealistic overshoot problems that can occur with the standard cubic spline and linear interpolation procedures. They suggested that the inability of linear interpolation to adequately incorporate the curvature of temperature profiles in the vertical (decreasing vertical temperature gradient in the upper thermocline) may result in overestimates of ocean heat content in pre-Argo periods and thus underestimate the temporal evolution of ocean heat content over recent decades as the vertical sampling increased with improved observational techniques.

Here, we assess Barker and McDougall's (2020) hypothesis by testing the sensitivity of global and regional upper (surface to 700 db) ocean heat content and thermosteric sea-level changes since the late 1950s to the vertical interpolation techniques and derive a new

observationally based estimate of global and regional upper ocean heat storage. We also test the sensitivity of the estimates to including or excluding XBT observations and recommend an approach for calculating time series of steric, thermosteric and halosteric sea-level change.

2. Data and variables and methods

We compare historical observations to a modern seasonal climatology developed for a period when there is virtually complete and relatively constant global coverage, as recommended by Cheng and Zhu (2014a). The reference period starts in 2006, as prior to this there are gaps in southern hemisphere coverage by Argo floats, and extends to the end of 2019 (centred on January 2013). We focus on ocean heat content in the upper 700 db because (i) the majority of the heat storage occurs there, (ii) the greater density of observations above this depth prior to the start of the Argo project, and (iii) because this is the part of the ocean water column with greater curvature in ocean properties versus depth. Our near global estimates are obtained by only integrating over parts of the ocean of depth greater than 700 m, thus not including continental shelves and some semi-enclosed marginal seas and excludes the Arctic Ocean north of 66ºN. The area included is 3.2×10^{14} m^2, about 89% of the global ocean areas, compared with 3.2×10^{14} m^2 for the Cheng and Zhu (2016) and 3.0×10^{14} m^2 for the von Schuckmann et al. (2020) estimates. If the ocean area not covered in our estimate, part of which is shallower than 700 db, has a similar heat storage per db to the area covered, we might underestimate the change by the order of 5-10%.

2.1 The data

The data set used is the quality-controlled EN4.2.2 data downloaded from the Met Office Hadley Centre website (in October 2021) for 1955 to 2020 (Good et al., 2013). EN4.2.2 is a compilation of four datasets: Argo, the Arctic Synoptic Basin-wide Oceanography (ASBO) project, the Global Temperature and Salinity Profile Programme (GTSPP), and the World Ocean Database 2018 (WOD18). We focus on the high quality hydrology (bottle data), CTD and Argo profiles.

We implemented additional quality control measures. For Argo data, we kept only delayed mode profiles to minimise problems of salinity drift in some real-time data. We followed the EN4.2.2 Product User Guide to keep casts whose QC_FLAGS_PROFILES is 0, eliminating duplicates and casts with suspicious temperature and salinity data. We also eliminated casts containing unrealistic SA and CT, eliminating, for example, 10% of the data in the 1970s.

After quality control, the selected profiles were converted into Absolute Salinity (S_A) and Conservative Temperature (Θ) by using gsw_SA_from_SP and gsw_CT_from_t functions from the Gibbs-Sea Water (GSW) Oceanographic Toolbox (McDougall and Barker 2011).

2.2 Vertical interpolation

The ocean heat content of the water column is evaluated by

$$\mathrm{OHC} = \sum \frac{c_p^0}{g}\,\Theta\,\delta P \qquad (1)$$

where c_p^0 is the specific heat capacity (gsw_cp0 from the GSW toolbox), g the acceleration due to gravity, Θ the Conservative Temperature and δP the pressure difference (in Pa) across the layer, with the sum being evaluated from the surface to the maximum pressure.

Our primary results for OHC anomalies and steric sea level changes use the Barker and McDougall (2020) Multiply-Rotated Piecewise Cubic Hermite Interpolation Polynomial (MR-PCHIP; referred to here as the MRST scheme when both temperature and salinity are interpolated jointly and MR when only a single variable is interpolated). We also computed the results for the linear LIN and RR methods and used the MR scheme for interpolating (i) temperature, replacing it the observed salinity data with a constant value (of 35.16504 g kg^{-1}, the Reference Salinity of Standard Seawater, IOC et al. 2010, but the result is not sensitive to the value used) and (ii) salinity. These interpolating methods are in the GSW Toolbox provided on theTEOS-10 website.

The vertical resolution is a key factor in the interpolation. The World Ocean Atlas (WOA) and Levitus levels have 16 and 41 discrete levels respectively in the upper 700 db of the water column. Here, we interpolate the data to a new level scheme whose vertical depth intervals vary in a geometric series with depth, starting with a resolution on 4 db near the surface with a total of 52 levels in the upper 700 db.

Tests comparing the regridded data with 623 one-db resolution CTD casts indicate that for the upper 700 db, each of the interpolation schemes result in errors of less than ±0.005ºC for virtually all levels of all casts when the original data was sampled at the above-mentioned geometric series of depths. For the Levitus levels, there were slightly greater errors, with

about 77% of the errors less than ±0.005ºC with the MRST and RR interpolation and 65% for the linear scheme. Virtually all errors were less than ±0.016ºC for all schemes, but a bias (interpolated minus 1 db data) to more positive errors was apparent with the linear scheme. For the WOA levels, there was a significant increase in errors. For MRST and RR, more than 60% of the errors were less than ±0.016ºC, but only 43% for linear interpolation. More importantly, while the errors for the MRST and RR schemes were roughly symmetrically distributed there was a significant bias for the linear scheme, with 64% of the errors greater than 0.005ºC, and with errors approaching 0.1ºC for a significant number of levels. (Note that a 0.005ºC temperature difference corresponds to about 5 ZJ for the upper 700 db of the global ocean.) The linear scheme imposes more positive biases on coarse resolution historical data and therefore underestimates the OHC trends in going from coarse resolution historical data to finer resolution recent data.

The sparse vertical sampling in some historical data results in a need for additional quality control tests. We discarded casts where adjacent observations in the upper 300 db have a vertical spacing greater than 100 db, eliminating a further 2% of the casts in the 1970s. The largest elimination of casts is a result of them not reaching 700 db, eliminating 70% of casts in the 1970s.

With the above quality control procedures, the MRST (and MR) and linear schemes were stable producing reasonable vertical integrals of ocean heat content and steric sea levels. However, in some (relatively rare) cases the RR scheme produced anomalous results and care was required to remove these casts from the global integrals.

191 *2.3 The seasonal climatology*

192

193 We estimate the reference climatology using an updated version of the four-dimensional
194 weighted least-squares ocean interpolation method of Dunn and Ridgway (2002) and
195 Ridgway et al. (2002) (as used in several recent studies, e.g. Durack and Wijffels, 2010;
196 Roemmich et al., 2015; and the CSIRO Atlas of Regional Seas, Ridgway et al., 2002) and
197 with high quality Argo, CTD and hydrology data. For a uniform 1° x 1° global grid, the
198 software uses all data located within an ellipse with a minimum radius of 300 km. This search
199 ellipse has a longitude-latitude ratio of 1.5 to 1, and expands until 400 data points are located
200 or the maximum radius is 1800 km. A least squares approach is used to estimate the central
201 value, the local spatial gradients and the annual and semi-annual seasonal cycles of upper
202 ocean heat content and steric sea level. When the data distribution is inadequate for loess
203 interpolation, we use a local interpolation from surrounding mapped values to fill the gaps.

204

205 *2.4 Historical OHC and Steric Changes*

206

207 Because of the sparse (in time and location) historical data, we group the vertically integrated
208 OHC and steric data into 11-year segments and 3-year segments (prior to 2006, then one year
209 segments after 2006), to minimise the impact of the sparse sampling. The number of
210 individual vertical heat content estimates for each 3 year/11-year period increases from about
211 34,000/123,000 in the 1970s, to 45,000/156,000 in the 1980s and then falling to
212 33,000/145,000 in the 1990s. These numbers increase rapidly after 2000 with the
213 implementation of Argo. After 2006, we utilise over 100,000 casts in the yearly estimates,
214 roughly equivalent to the number of historical casts in each of the historical 11 year periods.

For each historical epoch, the vertical integrals of the upper 700 db are compared with the equivalent seasonal climatologies (same location and day of year) and the changes between the data sets mapped using the same ocean lateral interpolation routine as used in developing the modern climatology. This mapping is completed with the anomalies rather than the absolute values to minimise aliasing from the large-scale spatial gradients into the differences between epochs and to minimise the impact of variable seasonal sampling. The mapped changes are integrated over the ocean area south of 66ºN that is deeper than 700 db to evaluate the global integrated ocean heat-content changes relative to the climatology.

2.5 Uncertainty and Bias Estimates

To estimate the uncertainties for each of the historical epochs prior to 2006, we subsampled 3-year segments of the Argo/WOD data in the reference period (12 segments from year 2007 to 2018) at the location and day of the year of the historical observations in the 3-year and 11-year segments. We then estimated the global ocean heat-content anomalies by comparing with the climatology and then mapping the anomalies. The resulting estimates were then compared with that estimated with the full Argo/WOD data set for the 3-year period (ensuring high density data coverage). These differences are an estimate of the effect of the limited temporal and spatial resolution of the data in the 3-year and 11-year intervals in the historical data. Twice the root-mean-square difference between the estimates with the subsampled and full data set is taken as an estimate of the 95% uncertainty. There are also smaller mean biases between the two estimates. After 2007, we compared each individual year with the same three-year segments as used for the historical data. This methodology is

similar to the approach of Cheng and Zhu (2016), except we map the anomalies with the four-dimensional weighted least-squares ocean interpolation scheme of Ridgeway et al. (2002) and compare with a data rich observational period, rather than model results.

3. Sensitivity of Global Ocean Heat Content Changes

The ocean heat content time series calculated with ocean station data only (bottle and CTD and Argo data only) (Figure 1a) for the yearly time series from 1956 to 2020 for the MRST and MR vertical interpolation schemes are essentially identical (differing by only 0.18 ZJ at most, rms 0.11 ZJ for the 3-year time series). The RR time series is also similar to the MRST and MR schemes with a rms difference of only 3.05 ZJ.

The ocean heat content increases from 1956 to the early 1960s and then decreases until about 1970 and then increases to 2020, for a total increase in ocean heat content of about 285 ZJ from 1956. The linear vertical interpolation displays similar interannual variability to the MRST, MR and RR schemes, but diverges prior to the 1990s such that the total heat-content increase is about 40 ZJ (about 14%) less over the record. For each interpolation scheme, the 11-year time series have much smaller mapping uncertainties and clearly reveal the time dependent bias when linear interpolation is used.

Our 95% uncertainty estimates for the 3-year time series from the incomplete sampling (Figure 1d) are about ±5 ZJ (not including instrumental accuracy) after 2000 but are larger, up to about ±25 ZJ, with the less dense sampling in the earlier part of the record around 1960, and there is a period of larger uncertainty in the second half of the 1990s. After 2002, the

mean bias of our 12 estimates are up to about ± 2 ZJ (corresponding to a mean temperature bias of about ± 0.002º C). The largest biases are a positive bias of about +4 ZJ in 1957 and a negative bias of about -18 ZJ in 1980. The mapping uncertainties and biases in the 11-year time series are small, less than ±6 ZJ.

The MRST/MR/RR heat contents are similar overall to the Cheng and Zhu (2016) time series (the IAP product), obtained by combining information from CMIP5 models with observations (Figure 1d). Our uncertainty estimates are slightly larger than those of Cheng and Zhu (2016) after 2000 and of similar magnitude prior to 1990. The two time series mostly overlap within the 95% uncertainty estimates (Figure 1d). The major exception is during the 1980s when the Cheng and Zhu is cooler by order 40 ZJ, corresponding to a mean temperature offset of about 0.04º C between the two time series. We note that during this period the Cheng et al. (2018; Figure 5) XBT bias corrections (to be subtracted from the XBT data) are larger than many other XBT corrections by up to 0.1º C (corresponding to almost 100 ZJ for 700 db).

The MRST and Cheng and Zhu (2016) have about a 60 ZJ larger increase in ocean heat content from the 1960s to the end of the record than the ensemble average of 15 estimates reported by von Schuckmann et al. (2020). Their uncertainties are generally larger, particularly, around 1980 and 2000, and there is some limited overlap of the 95% uncertainty estimates prior to 1990.

3.1 The sensitivity to inclusion of XBTs

Including XBTs with the Gouretski and Reseghetti (2010) corrections resulted in lower heat content estimates, with the largest differences from 1980 to 2000, peaking at almost 40 ZJ (corresponding to cooler estimated global temperatures of about 0.04º C) in 1991. The Cheng et al. (2014) corrections resulted in heat content estimates similar to our estimates excluding XBTs estimates after the early 1990s (and greater than using the Gouretski and Reseghetti corrections by about 25 ZJ in the early 1990s) but were lower than our non XBT estimates prior to the early 1990s, with the largest difference of about 25 ZJ (corresponding to global temperature differences of 0.025º C) in the mid to late 1980s.

These differences are similar to the twice standard deviation between corrected XBT data and the reference data sets used in developing the XBT corrections that range from ± 0.03 º C to ± 0.06 º C (corresponding to ± 30 ZJ to ± 60 ZJ) for the four favored XBT corrections with the EN data (Cheng et al., 2018; Table 1, Figure 5). These XBT biases are systematic and cannot be eliminated by improved historical data coverage or mapping methods. However, the mapping uncertainties in the global estimates can be reduced by greater temporal averaging. Because these XBT corrections are both significant and uncertain, we argue that further refinement of the corrections is required to reduce the uncertainties significantly. As a result, we prefer to focus on decadal time series evaluated from vertical casts that contain higher quality temperature and salinity data, without using the XBT data.

4. Sensitivity of Global Mean Steric Sea-level Changes

Changes in mean sea level arise from (i) the addition of mass to the ocean (principally from land-based ice), and (ii) the increasing temperature of the ocean (ocean thermosteric sea-level

change). Since the total amount of salt in the ocean is unchanged by this addition of mass and the haline contraction coefficient is almost constant, any (subsequent) mixing of the additional freshwater with existing ocean water has negligible impact on global mean sea level (Gregory et al., 2019). That is, the global mean steric sea-level rise is the thermosteric sea-level rise and the global mean steric sea-level change from changes in the interior distribution of salinity is nearly zero. Here, we concentrate on the best methods for estimating the thermosteric sea level rise and ignore the changes in sea level caused by the addition of mass.

Ocean thermosteric sea-level changes are directly caused by temperature changes. We could evaluate this thermosteric sea-level rise by using the first order Taylor expansion:

$$\Delta\eta_{\Theta}(x,y) = \sum \Delta\Theta \frac{\partial v}{\partial \Theta}\left(\frac{1}{2}[\Theta^{i}+\Theta^{r}], \frac{1}{2}[S_{\mathrm{A}}^{i}+S_{A}^{r}], p\right)\frac{\delta P}{g}. \quad (2)$$

However, we prefer the finite amplitude definitions of thermosteric and halosteric sea-level change:

$$\Delta\eta_{\Theta}(x,y) = \sum \frac{1}{2}\left\{v\left(\Theta^{i},S_{A}^{i},p\right)-v\left(\Theta^{r},S_{A}^{i},p\right)+v\left(\Theta^{i},S_{A}^{r},p\right)-v(\Theta^{r},S_{A}^{r},p)\right\}\frac{\delta P}{g} \quad (3)$$

and

$$\Delta\eta_{\mathrm{S}}(x,y) = \sum \frac{1}{2}\left\{v\left(\Theta^{i},S_{A}^{i},p\right)-v\left(\Theta^{i},S_{A}^{r},p\right)+v\left(\Theta^{r},S_{A}^{i},p\right)-v(\Theta^{r},S_{A}^{r},p)\right\}\frac{\delta P}{g}, \quad (4)$$

where v is the specific volume, *i* indicates the historical epoch and *r* the reference period and the summation is over the depth of the water column considered. With these definitions the total steric change is exactly the sum of the thermosteric and halosteric contribution:

$$\Delta\eta(x,y) = \Delta\eta_{\Theta}(x,y)+\Delta\eta_{\mathrm{S}}(x,y) = \sum\left\{v\left(\Theta^{i},S_{A}^{i},p\right)- v(\Theta^{r},S_{A}^{r},p)\right\}\frac{\delta P}{g}, \quad (5)$$

333 so that if the specific volumes of the initial and final water parcels are identical there is no
334 contribution to sea level change. This is not the case when the linearized thermal expansion
335 and haline contraction coefficients are used to estimate the thermosteric and halosteric
336 contributions to sea level change, as in Eqn. (2).
337
338 The global mean thermosteric sea level (Figure 1b) increases to 1960, then decreases to 1970
339 followed by an ongoing trend to the end of the record, similar to the global ocean heat
340 content increase. The LIN interpolation underestimates the MRST increase by about 14%
341 since 1956, with the two linear trends of 0.48 and 0.55 mm yr^{-1}. Note the thermosteric sea
342 level curve has a zero crossing in 2010 and is about +1.5 mm at the middle of the reference
343 period. This offset is because for the reference period the temperature and salinity have been
344 mapped separately resulting in a lower thermosteric sea level (Gille, 2004). However, this
345 cabbeling does not affect the time series as the only mapping at each epoch is of the
346 thermosteric sea level anomalies.
347
348 The halosteric sea level (Figure 1c) has a rms variability of 4 mm (consistent with our
349 inability to measure global averaged salinity to better than 0.01) for the 3-year averages and 1
350 mm for the 11-year averages. There is a significant negative spike at the end of the record
351 indicative of biases in the Argo salinity data. There is slight divergence between the MRST
352 and LIN estimates of the global mean halosteric contribution.
353
354 **5. Sensitivity of Regional Ocean Heat Content and Steric Sea-level Trends**
355

356 The horizontal distribution of ocean heat-content linear trends over 1970 to 2014, expressed
357 here as an equivalent surface flux to allow comparison with other products (e.g. Johnson and
358 Lyman, 2020), are very similar for the four vertical interpolation methods, and hence only the
359 MRST heat content changes are shown (Figure 2a). The main features are a greater warming
360 and thermosteric sea-level trends (Figure S1 in Supporting Information) in the Atlantic Ocean
361 (particularly the North Atlantic) than the Pacific or Indian Oceans, maxima at the poleward
362 edges of the subtropical gyres in both hemispheres (consistent with the spin-up and/or the
363 poleward expansion of the subtropical gyres) and positive heat storage and thermosteric sea
364 level in the western and northern Indian Ocean (north of about 10º S, the latitude the Pacific
365 Indian throughflow enters the Indian Ocean). There are areas of lower heat storage and
366 thermosteric sea level between the equator and about 20º S in the Pacific and Indian Oceans.
367 Similar patterns can be seen in the three maps for a similar period reported by Johnson and
368 Lyman (2020), with Figure 2a most similar to the maps from the National Centre for
369 Environmental Information. The zonal integrals (Figure 2c) indicate a maxima near the
370 poleward boundaries of the subtropical gyres and less accumulated heat at both lower and
371 higher latitudes. The thermosteric sea-level trends are similar except that they are larger in
372 the northern hemisphere (Figure 2a, Figure S1).
373
374 There are systematic differences in the pattern between the MRST and the LIN vertical
375 interpolation methods for both heat content (Figure 2b) and thermosteric and halosteric sea-
376 level trends (Figure S1). The LIN interpolation underestimates the changes at lower latitudes.
377 The heat content underestimates peak near 15ºN and S at about 100% and 50% of the zonal
378 averages at these latitudes and about 12% of the maximum trend at 40ºS. For thermosteric sea
379 level, the underestimates peak near 17ºN and 12ºS at about 25% and 80% of the zonal

averages at these latitudes. This pattern arises because the linear vertical interpolation scheme cannot adequately reproduce the curvature in the temperature-depth profile in the sparse vertical resolution of the historical data that is largest at lower latitudes in the sub-tropical gyres where the upper ocean water column is more highly stratified.

The halosteric trends are smaller than the thermosteric trends and are negative in the North Atlantic and the western and northern Indian Ocean (consistent with salinification) and negative in the Pacific Ocean and the Southern Ocean (consistent with freshening). The difference between the MRST and LIN trends are small but reveal systematic spatial trends with a negative halosteric bias in the subtropical gyres (the linear interpolation is unable to adequately represent the upper ocean salinity maxima in historical observations) and a slight positive bias at high latitudes.

6. Discussion and Conclusions

We have shown the time-dependent vertical resolution of the historical data sets combined with the linear vertical interpolation rather than Multiply-Rotated Piecewise Cubic Hermite Interpolating Polynomials (MRST-PCHIP) (Barker and McDougall, 2020) underestimates the trends in upper 700 db ocean heat content by 40 ZJ (almost 14%) over the historical record and by about 14% for ocean thermal expansion. The Reiniger and Ross (1968) technique produces similar results to the MRST-PCHIP methods, but we note it has a greater tendency to produce artificial anomalous water properties (Barker and McDougall, 2020) and in some circumstances is difficult to apply, producing unrealistic results, as also found by others (Johnson et al., 2011).

Our upper ocean heat content time series is dependent on observations alone, with no recourse to model results for interpolation between data points, or on an initial estimate, and thus may be more suitable for detection and attribution studies. It indicates a similar increase to that of Cheng and Zhu (2016) but larger than the ensemble average estimate of von Schuckmann et al. (2020). We found differences between different XBT corrections were of similar magnitude to the differences between only using high quality hydrographic data and also including XBT data, and our mapping uncertainties. It would appear that further refinement of XBT corrections is required for XBTs to provide stronger constraints on global ocean heat content. As a result, we focused on decadal time series (with smaller uncertainties) evaluated from vertical casts that only contain higher quality temperature and salinity data. For comparison with the reporting periods and methods used in von Schuckmann et al. (2022), we use the heat content from the smoothed time series for the start of the record and the Argo value in 2020. For the ocean area considered, the heat content increases for 1960-2020, 1971-2020, 1993-2020 and 2006-2020 are 242 ZJ (0.40 W m^{-2}), 259 ZJ (0.52 W m^{-2}), 193 ZJ (0.71 W m^{-2}) and 107 ZJ (0.75 W m^{-2}), near the upper end of the ranges in von Schuckmann et al.

This apparently simple issue of vertical interpolation of ocean temperature profiles with time-varying resolution has significant implications. In estimating ocean heat content changes, Bagnell and DeVries (2021) used linear interpolation of temperature profiles. Our results indicate their approach may underestimate the ocean heat content increase in the upper 700 m by the order of 40 ZJ prior to 1990. This additional warming for the upper 700 m implied by a more realistic vertical interpolation scheme would more than offset the deep (greater than

2000 m) ocean cooling of 30 ZJ over 1945 to 1990 reported by Bagnell and DeVries (2021). Adding this potential bias would bring their ocean heat content changes more in line with objective mapping techniques (e.g. Cheng et al., 2017) and would substantially alter their conclusion of no ocean heat content increases prior to 1990. Although there is less curvature in the temperature profiles over the larger depth range between 700 m and 2000 m and below, there is generally sparser vertical sampling in the historical data. As a result, the potential biases of ocean heat content increase from 700 m to 2000 m (and possibly below) prior to 1990 may be similar to our estimate for the upper 700 m.

While the spatial trends are similar with all schemes, the use of linear vertical interpolation shows a clear spatial pattern of underestimating ocean heat content and thermosteric sea-level rise in the low latitudes of the subtropical gyres. These differences may be important in evaluating ocean and climate models and for the detection and attribution of climate change.

We recommend the stable and easily implemented Multiply-Rotated Piecewise Cubic Hermite Interpolating Polynomials as a standard tool for vertical interpolation to minimise biased results associated with the linear interpolation scheme and the difficulties with the Reiniger and Ross technique. The appropriate software is available on the TEOS-10 website.

Acknowledgements:

J.C. and Y.L. were supported by the Centre for Southern Hemisphere Oceans Research (CSHOR), jointly funded by the Qingdao National Laboratory for Marine Science and Technology (QNLM, China) and the Commonwealth Scientific and Industrial Research

Organisation (CSIRO, Australia), and the Australian Research Council's Discovery Project funding scheme (project DP190101173). TMcD and PMB gratefully acknowledge Australian Research Council support through grant FL150100090. This paper contributes to the tasks of the Joint SCOR/IAPSO/IAPWS Committee on the Thermophysical Properties of Seawater.

Data and Software Availability:

The data used in this study is the publicly available ocean observations in the ENACT data set (EN4.2.2; Good et al. 2013) and were downloaded in October 2021. EN.4.2.2 data were obtained from https://www.metoffice.gov.uk/hadobs/en4/ and are © British Crown Copyright, Met Office, [2021], provided under a Non-Commercial Government Licence http://www.nationalarchives.gov.uk/doc/non-commercial-government-licence/version/2/. https://www.metoffice.gov.uk/hadobs/en4/download-en4-2-2.html. The equation of state routines and the interpolation methods are available at the TEOS 10 Oceanographic Toolbox Website (https://www.teos-10.org/pubs/gsw/html/gsw_contents.html). The MR-PCHIP interpolation algorithm of this paper is available as the functions gsw_tracer_interp and gsw_t_interp; these programs are designed for use with in situ observations where salinity has not been recorded. The MRST-PCHIP is available in the programs gsw_SA_CT_interp and gsw_ tracer_CT_interp. More information on the mapping is given in the the CARS papers (Dunn and Ridgway, 2002; Ridgway et al. 2002) (http://www.marine.csiro.au/~dunn/cars2009/). The time series of ocean heat content changes and the regional distributions presented in Figures 1a, 1b, 1d, 2 and S1 will be available at the TEOS-10 website.

476 **References**

477 Bagnell, A., and T. DeVries (2021), 20th century cooling of the deep ocean contributed to
478 delayed acceleration of Earth's energy imbalance, *Nature Communications*, *12*(1), 4604.
479 Barker, P. M., and T. J. McDougall (2020), Two Interpolation Methods Using Multiply-
480 Rotated Piecewise Cubic Hermite Interpolating Polynomials, *Journal of Atmospheric and*
481 *Oceanic Technology*, *37*(4), 605-619.
482 Bindoff, N.L., J. Willebrand, V. Artale, A, Cazenave, J. Gregory, S. Gulev, K. Hanawa, C.
483 Le Quéré, S. Levitus, Y. Nojiri, C.K. Shum, L.D. Talley and A. Unnikrishnan (2007)
484 Observations: Oceanic Climate Change and Sea Level. In: Climate Change 2007: The
485 Physical Science Basis. Contribution of Working Group I to the Fourth Assessment
486 Report of the Intergovernmental Panel on Climate Change [Solomon, S., D. Qin, M.
487 Manning, Z. Chen, M. Marquis, K.B. Averyt, M. Tignor and H.L. Miller (eds.)].
488 Cambridge University Press, Cambridge, United Kingdom and New York, NY, USA.
489 Boyer, T., et al. (2016), Sensitivity of Global Upper-Ocean Heat Content Estimates to
490 Mapping Methods, XBT Bias Corrections, and Baseline Climatologies, *Journal of*
491 *Climate*, *29*(13), 4817-4842.
492 Cheng, L., and J. Zhu (2014a), Influences of the Choice of Climatology on Ocean Heat
493 Content Estimation, *Journal of Atmospheric and Oceanic Technology*, *32*(2), 388-394.
494 Cheng, L., and J. Zhu (2014b), Uncertainties of the Ocean Heat Content Estimation Induced
495 by Insufficient Vertical Resolution of Historical Ocean Subsurface Observations, *Journal*
496 *of Atmospheric and Oceanic Technology*, *31*(6), 1383-1396.
497 Cheng, L., and J. Zhu (2016), Benefits of CMIP5 Multimodel Ensemble in Reconstructing
498 Historical Ocean Subsurface Temperature Variations, *Journal of Climate*, *29*(15), 5393-
499 5416.

Cheng, L., J. Zhu, R. Cowley, T. Boyer, and S. Wijffels (2014), Time, Probe Type, and Temperature Variable Bias Corrections to Historical Expendable Bathythermograph Observations, *Journal of Atmospheric and Oceanic Technology*, *31*(8), 1793-1825.

Cheng, L., K. E. Trenberth, J. Fasullo, T. Boyer, J. Abraham, and J. Zhu (2017), Improved estimates of ocean heat content from 1960 to 2015, *Science Advances*, *3*(3).

Cheng, L., H. Luo, T. Boyer, R. Cowley, J. Abraham, V. Gouretski, F. Reseghetti, and J. Zhu (2018), How Well Can We Correct Systematic Errors in Historical XBT Data?, *Journal of Atmospheric and Oceanic Technology*, *35*(5), 1103-1125.

Church, J. A., N. J. White, L. F. Konikow, C. M. Domingues, J. G. Cogley, E. Rignot, J. M. Gregory, M. R. van den Broeke, A. J. Monaghan, and I. Velicogna (2011), Revisiting the Earth's sea-level and energy budgets from 1961 to 2008, *Geophys. Res. Lett.*, *38*(18), L18601.

Church, J. A., N. J. White, L. F. Konikow, C. M. Domingues, J. Graham Cogley, E. Rignot, J. M. Gregory, M. R. van den Broeke, A. J. Monaghan, and I. Velicogna (2013a), Correction to “Revisiting the Earth's sea-level and energy budgets from 1961 to 2008”, *GEOPHYSICAL RESEARCH LETTERS*, *40*(15), 4066-4066.

Church, J. A., et al. (2013b), Sea Level Change, in *Climate Change 2013: The Physical Science Basis. Contribution of Working Group I to the Fifth Assessment Report of the Intergovernmental Panel on Climate Change*, edited by T. F. Stocker, D. Qin, G.-K. Plattner, M. Tignor, S.K. Allen, J. Boschung, A. Nauels, Y. Xia, V. Bex and P.M. Midgley, Cambridge University Press, Cambridge, United Kingdom and New York, NY, USA.

522 Domingues, C. M., J. A. Church, N. J. White, P. J. Gleckler, S. E. Wijffels, P. M. Barker, and
523 J. R. Dunn (2008), Improved estimates of upper-ocean warming and multi-decadal sea-
524 level rise, *Nature*, **453**(7198), 1090-1093.
525 Dunn J.R., and K.R. Ridgway (2002), Mapping ocean properties in regions of complex
526 topography, *Deep Sea Research I: Oceanographic Research*, **49(3)**, 591-604.
527 Forster, P., T. Storelvmo, K. Armour, W. Collins, J.-L. Dufresne, D. Frame, D.J. Lunt, T.
528 Mauritsen, M.D. Palmer, M. Watanabe, M. Wild, and H. Zhang (2021), The Earth's
529 Energy Budget, Climate Feedbacks, and Climate Sensitivity. In *Climate Change 2021:*
530 *The Physical Science Basis. Contribution of Working Group I to the Sixth Assessment*
531 *Report of the Intergovernmental Panel on Climate Change* [Masson-Delmotte, V., P. Zhai,
532 A. Pirani, S.L. Connors, C. Péan, S. Berger, N. Caud, Y. Chen, L. Goldfarb, M.I. Gomis,
533 M. Huang, K. Leitzell, E. Lonnoy, J.B.R. Matthews, T.K. Maycock, T. Waterfield, O.
534 Yelekçi, R. Yu, and B. Zhou (eds.)]. Cambridge University Press, Cambridge, United
535 Kingdom and New York, NY, USA, pp. 923–1054, doi:10.1017/9781009157896.009.
536 Durack, P. J., and S. E. Wijffels (2010), Fifty-Year Trends in Global Ocean Salinities and
537 Their Relationship to Broad-Scale Warming, *Journal of Climate*, *23*(16), 4342-4362.
538 Gille, S. T. (2004), How nonlineraities in the equation of state of sea water can confound
539 estimates of steric sea level change, *Journal of Geophysical Research*, *109*, C03005,
540 doi:03010.01029/02003JC002012.
541 Good, S. A., M. J. Martin and N. A. Rayner (2013), EN4: quality controlled ocean
542 temperature and salinity profiles and monthly objective analyses with uncertainty
543 estimates, *Journal of Geophysical Research: Oceans*, **118**, 6704-
544 6716, doi:10.1002/2013JC009067

545 Gould, J., and T. A. S. Team (2004), Argo Profiling Floats Bring New Era of In Situ Ocean
546 Observations, *EoS, Transactions of the American Geophysical Union*, *85*(19, 11 May).
547 Gouretski, V., and K. P. Koltermann (2007), How much is the ocean really warming?,
548 *GEOPHYSICAL RESEARCH LETTERS*, *34*(1), L01610.
549 Gouretski, V., and F. Reseghetti (2010), On depth and temperature biases in
550 bathythermograph data: Development of a new correction scheme based on analysis of a
551 global ocean database, *Deep Sea Research Part I: Oceanographic Research Papers*,
552 *57*(6), 812-833.
553 Gregory, J. M., et al. (2019), Concepts and Terminology for Sea Level: Mean, Variability and
554 Change, Both Local and Global, *Surveys in Geophysics*, *40*(6), 1251-1289.
555 IOC, SCOR and IAPSO: The international thermodynamic equation of seawater – 2010:
556 Calculation and use of thermodynamic properties. Intergovernmental Oceanographic
557 Commission, Manuals and Guides No. 56, UNESCO (English), 196 pp. available at
558 http://www.TEOS-10.org/pubs/TEOS-10_Manual.pdf Many of the original papers on
559 which TEOS-10 is based were published in the following Special Issue of Ocean Science,
560 https://os.copernicus.org/articles/special_issue14.html 2010.
561 Ishii, M., and M. Kimoto (2009), Reevaluation of historical ocean heat content variations
562 with time-varying XBT and MBT depth bias corrections, *Journal of Oceanography*, *65*(3),
563 287-299.
564 Ishii, M., M. Kimoto, K. Sakamoto, and S.-I. Iwaski (2005), Historical ocean subsurface
565 temperature analysis with error estimate - revisited, *Monthly Westher Review*.
566 Johnson, D. R., T. P. Boyer, H. E. Garcia, R. A. Locarnini, O. K. Baranova, and M. M.
567 Zweng, 2011: World Ocean Database 2009 documentation. NODC Internal Rep. 20, 175
568 pp., http://www.nodc.noaa.gov/OC5/WOD09/pr_wod09.html.

569 Johnson, G. C., and J. M. Lyman (2020), Warming trends increasingly dominate global
570 ocean, *Nature Climate Change*, **8**, 757-761.
571 Johnson, G. C., J. M. Lyman, and N. G. Loeb (2016), Improving estimates of Earth's energy
572 imbalance, *Nature Clim. Change*, *6*(7), 639-640.
573 Levitus, S., J. Antonov, and T. Boyer (2005), Warming of the world ocean, 1955-2003,
574 *Geophys. Res. Lett.*, *32*, L02604.
575 Levitus, S., J. Antonov, J. Wang, T. Delworth, K. Dixon, and A. Broccoli (2001),
576 Anthropogenic warming of Earth's climate system, *Science*, *292*(5515), 267-270.
577 Levitus, S., J. I. Antonov, T. P. Boyer, R. A. Locarnini, H. E. Garcia, and A. V. Mishonov
578 (2009), Global ocean heat content 1955-2007 in light of recently revealed instrumentation
579 problems, *Geophysical Research Letters*, *36*, L07608, doi:07610.01029/02008GL037155.
580 McDougall, T.J. and P.M. Barker, 2011: Getting started with TEOS-10 and the Gibbs
581 Seawater (GSW) Oceanographic Toolbox, 28pp., SCOR/IAPSO WG127, ISBN 978-0-
582 646-55621-5.
583 Murphy, D. M., S. Solomon, R. W. Portmann, K. H. Rosenlof, P. M. Forster, and T. Wong
584 (2009), An observationally based energy balance for the Earth since 1950, *J. Geophys.*
585 *Res.*, *114*(D17), D17107.
586 Reiniger, R. F., and C. K. Ross (1968), A method of interpolation with application to
587 oceanographic data, *Deep Sea Research and Oceanographic Abstracts*, *15*(2), 185-193.
588 Rhein, M., S.R. Rintoul, S. Aoki, E. Campos, D. Chambers, R.A. Feely, S. Gulev, G.C.
589 Johnson, S.A. Josey, A. Kostianoy, C. Mauritzen, D. Roemmich, L.D. Talley and F. Wang
590 (2013), Observations: Ocean, in *Climate Change 2013: The Physical Science Basis.*
591 *Contribution of Working Group I to the Fifth Assessment Report of the Intergovernmental*
592 *Panel on Climate Change*, edited by T. F. Stocker, D. Qin, G.-K. Plattner, M. Tignor, S.K.

593 Allen, J. Boschung, A. Nauels, Y. Xia, V. Bex and P.M. Midgley, pp. 255–316,
594 Cambridge University Press, Cambridge, United Kingdom and New York, NY, USA.
595 Ridgway, K. R., J. R. Dunn, and J. L. Wilkin (2002), Ocean interpolation by four-
596 dimensional weigted least squares - Applications to the waters around Australasia, *Jouranl*
597 *of Atmospheric and Oceanic Technology*, *19*(September), 1357-1375.
598 Roemmich, D., J. Church, J. Gilson, D. Monselesan, P. Sutton, and S. Wijffels (2015),
599 Unabated planetary warming and its ocean structure since 2006, *Nature Clim. Change*,
600 *5*(3), 240-245.
601 Savita, A., Catia M. Domingues, Tim Boyer, Viktor Gouretski, Masayoshi Ishii, Gregory C.
602 Johnson, John M. Lyman, Josh K. Willis, Simon J. Marsland, William Hobbs, John A.
603 Church, Didier P. Monselesan, Peter Dobrohotoff, Rebecca Cowley and Susan E. Wijffels.
604 (2022) Quantifying uncertainty in spatio-temporal changes of upper-ocean heat content
605 estimates: an internationally coordinated comparison. *Journal of Climate*, **35**, 851-875.
606 https://doi.org/10.1175/JCLI-D-20-0603.1
607 Stephens, G. L., J. Li, M. Wild, C. A. Clayson, N. Loeb, S. Kato, T. L'Ecuyer, P. W.
608 Stackhouse, M. Lebsock, and T. Andrews (2012), An update on Earth's energy balance in
609 light of the latest global observations, *Nature Geosci*, *5*(10), 691-696.
610 Trenberth, K. E., and J. T. Fasullo (2010), Tracking Earth's Energy, *Science*, *328*(5976), 316-
611 317.
612 von Schuckmann, K., et al. (2016), An imperative to monitor Earth's energy imbalance,
613 *Nature Clim. Change*, *6*(2), 138-144.
614 von Schuckmann, K., et al. (2020), Heat stored in the Earth system: where does the energy
615 go?, *Earth Syst. Sci. Data*, *12*(3), 2013-2041.

616 von Schuckmann, K., et al. (2022), Heat stored in the Earth system: where does the energy
617 go?, *Earth Syst. Sci. Data Discussions*, https://doi.org/10.5194/essd-2022-239.
618 Wijffels, S., D. Roemmich, D. Monselesan, J. Church, and J. Gilson (2016), Ocean
619 temperatures chronicle the ongoing warming of Earth, *Nature Clim. Change*, *6*(2), 116-
620 118.
621 Wijffels, S., J. Willis, C. Domingues, P. Barker, N. White, A. Gronell, K. Ridgway, and J.
622 Church (2008), Changing Expendable Bathythermograph Fall Rates and Their Impact on
623 Estimates of Thermosteric Sea Level Rise, *Journal of Climate*, *21*(21), 5657-5672.
624

Figures

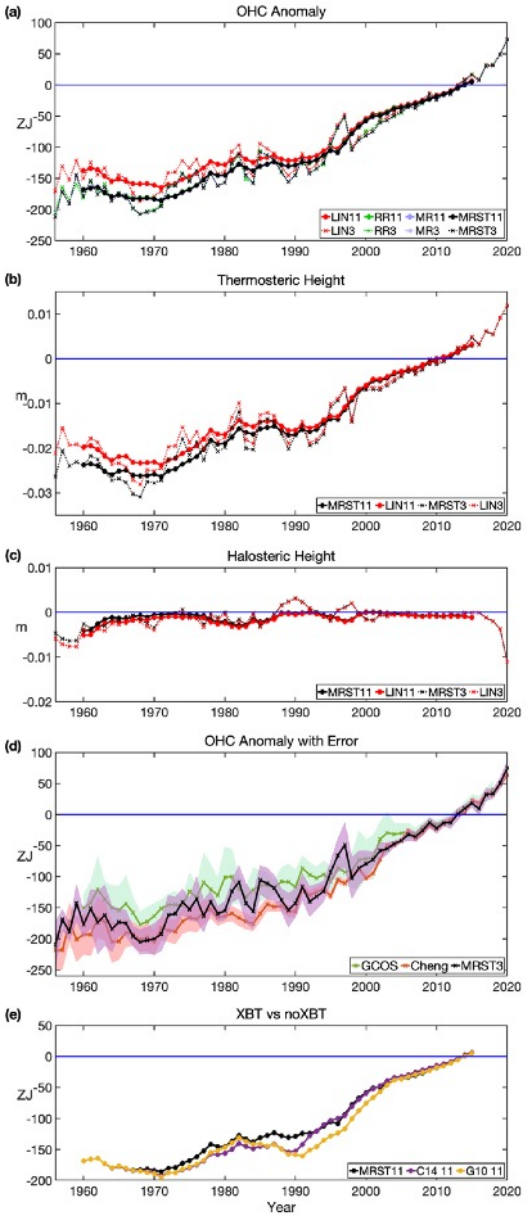

Figure 1. Upper ocean (to 700 db) heat content (a), thermosteric (b) and halosteric (c) sea level change for the vertical interpolation schemes (Linear red, RR green, MR blue, MRST black). For (a-c), the 3-year time series from 1956 to 2020) are indicated by the dotted lines and the 11-year time series (from 1960 to 2015) are the solid lines. (d) Time series of the upper 700 db ocean heat content for the MRST interpolation compared to the estimates from Cheng and Zhu (2016, red) and von Schuckmann et

al. (2020, green (GCOS)). The 95% uncertainty estimates are indicated by the shading. (e) The MRST 11-year time series with no XBTs (black), XBT data with the Gouretski and Reseghetti (G10, yellow) and Cheng corrections (C14, purple).

Figure 2

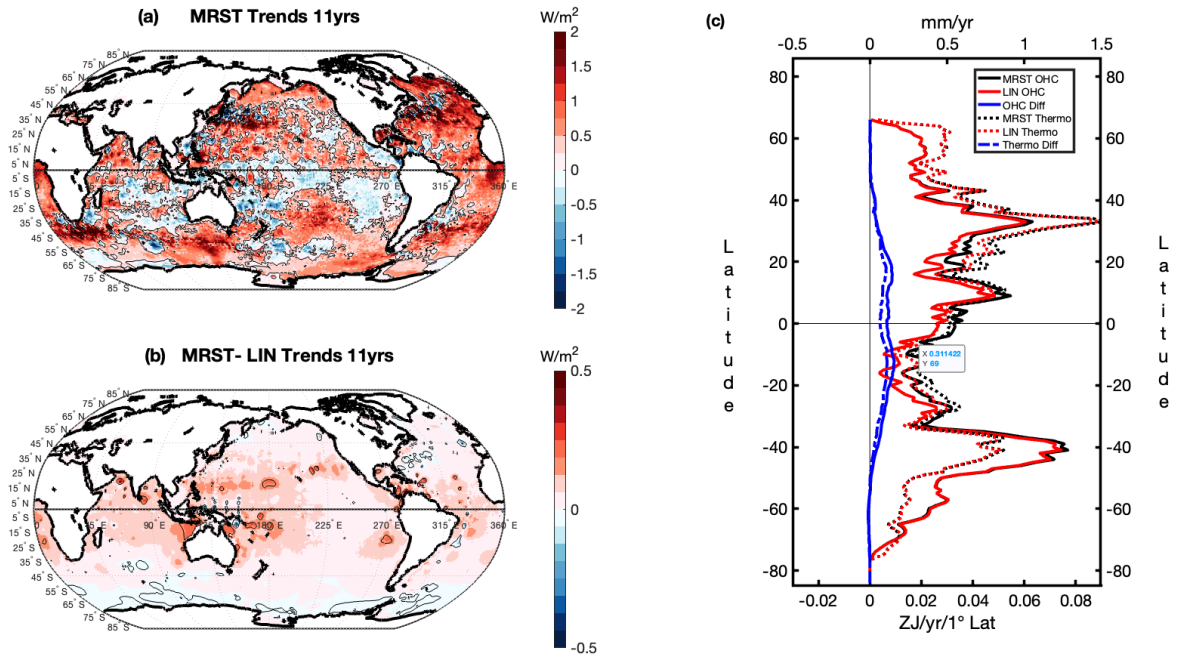

Figure 2. Ocean Heat Content trends in the upper 700 m for 1970 to 2015. (a) The equivalent surface flux into the ocean in W m^{-2}, (b) the differences between the MRST and Linear vertical interpolation equivalent surface flux into the ocean in W m^{-2}, and (c) the zonal integral of the accumulated heat content in Zeta Joules per degree latitude per year (MRST black and LIN red, and their differences blue). The dashed black and red lines show the zonally integrated thermosteric in mm per year (upper axis).